Plasmonics (2022) 17:193–201
https://doi.org/10.1007/s11468-021-01509-3

Silver Nanoparticles Textured Oxide Thin Films for Surface Plasmon Enhanced Photovoltaic Properties

Amitabha Nath[1] · Naveen Bhati[1,2,4,5] · Bikram Kishore Mahajan[3] · Jayanta Kumar Rakshit[1,4] · Mitra Barun Sarkar[1]

Received: 5 May 2021 / Accepted: 26 July 2021 / Published online: 3 August 2021

Abstract

In this report, Ag nanoparticles were fabricated using the single-step glancing angle deposition (SS-GLAD) technique upon In_2O_3/TiO_2 thin film. Afterward, a detailed analysis was done for the two samples such as In_2O_3/TiO_2 thin film and In_2O_3/TiO_2 thin film/Ag nanoparticles, to inspect the field emission scanning electron microscopy (FESEM), energy-dispersive X-ray analysis (EDAX), X-ray diffraction (XRD), ultraviolet (UV) spectroscopy, and electrical properties. The reduction in bandgap energy for the samples of In_2O_3/TiO_2 thin film/Ag nanoparticles (~4.16 eV) in comparison with the In_2O_3/TiO_2 thin film (~4.28 eV) was due to trapped *e–h* recombination at the oxygen vacancies and electron transmission of Ag to the conduction band of the In_2O_3/TiO_2 thin films. Moreover, under irradiation of photons Ag nanoparticles generated inorganic Ag–O compound attributable to the localized surface plasmon resonance (LSPR). Also, a ~90% high transmittance, ~60% and ~25% low reflectance in UV and visible region, fill factor (FF) of 53%, as well as power conversion efficiency (PCE) of 15.12% was observed for In_2O_3/TiO_2 thin film/Ag nanoparticles than the In_2O_3/TiO_2 thin film. Therefore, the use of Ag nanoparticles textured In_2O_3/TiO_2 thin film–based device is a promising approach for the forthcoming photovoltaic applications.

Keywords Thin films · Ag nanoparticles · Localized surface plasmon resonance · Photovoltaic properties

Introduction

With the growing world population, one of the greatest challenges our society is currently facing is that of clean energy. Solar energy, being abundant, presents itself as a lucrative solution and this led researchers all over the world in pursuit of various photovoltaic devices, which can convert sunlight to electrical energy for numerous applications. While the commercial solar panels are still predominantly manufactured from crystalline Silicon, researchers are exploring various materials, configurations, and fabrication techniques to develop highly efficient, inexpensive, and reliable photovoltaic devices. Among them dye-sensitized solar cells [1–3], perovskites [4, 5], quantum-dots [6–8], organic material-based solar cells [9, 10], etc., has been explored by various research groups around the world in the last couple of decades.

One of the primary objectives of the solar cell researchers in any material or configuration is to achieve high absorption of photons, which can lead to increased efficiency. To circumvent the limits posed by the 'diffusion length' of the charge carriers, researchers sometimes incorporate back side reflectors or attempt to 'trap' the photons inside device, which leads to increased photon path length or optical thickness. The later approach can be achieved by texturing the surface which can guide the scattered light within the active material, leading to longer photon path length and hence improved efficiency. A popular technique of texturing the surface is by depositing various shapes and sizes of metal nanoparticles. One of the first reports in this area was by Stuart and Hall [11], where silver nanoparticles

✉ Mitra Barun Sarkar
mbarun.ece@nita.ac.in

1 Department of Electronics and Communication Engineering, National Institute of Technology Agartala, Jirania 799046, India

2 Department of Electrical Engineering, National Institute of Technology Agartala, Jirania 799046, India

3 School of Electrical and Computer Engineering, Purdue University, West Lafayette, IN 47907, USA

4 Department of Electronics and Instrumentation Engineering, National Institute of Technology Agartala, Jirania 799046, India

5 Department of Electrical Engineering, Indian Institute of Technology Roorkee, Roorkee, Uttarakhand 247667, India

deposited on silicon-on-insulator (SOI) photodetector enhanced the photocurrent by an order of magnitude. This was achieved due to a phenomenon known as localized surface plasmon resonance (LSPR) [12–14]. LSPR is induced when the frequency of the incoming photon matches with that of the oscillating electrons of the nanoparticles, leading to an increased electromagnetic field which aids in light concentration around the nanoparticles. This phenomenon of guided light, coupled with strong light scattering due to the nanoparticles, has led to tremendous research interest in recent years and several nanoparticles, viz., gold (Au) [15–17], silver (Ag) [18–20], aluminium (Al) [21–23] etc., nanorods [24–26], nano discs [27, 28], has been explored, leading to high efficiency.

In addition to classical solar cells based on p–n junction, novel structures such as photoelectrochemical solar cells [29], and solar cells based non schottky diodes [30], metal–insulator-semiconductor (MIS) solar cells [31], semiconductor-insulator-semiconductor (SIS) solar cells [32], etc., have been explored by various research groups around the world. Among them, SIS structures showed enormous potential as low-cost photovoltaic devices. In SIS structures, instead of a p–n junction, the separation of charges are carried out by the electric field at the semiconductor-insulator interface. Several SIS structures (e.g., ITO/SiO*x*/p-Si, Al-SiO*x*/p-Si, PEDOT:PSS/c-Ge, etc.) has been fabricated and analysed since 1980s [32–34]. Combining the SIS structures with LSPR presents a lucrative approach to fabricate low-cost, high efficiency solar cells. In addition, one can also tailor the photovoltaic device to absorb the desired wavelengths in the solar spectrum, for specific applications. This can be achieved by a suitable choice of active materials to construct a multi-junction solar cell. Titanium dioxide (TiO_2) (E_g ~3.2 eV) and indium oxide (In_2O_3) (E_g ~3.6 eV) are some of the most extensively used materials due to their availability, ease of handling, low cost, non-toxicity, and its optoelectronic applications [35, 36]. By itself TiO_2 shows the properties of photovoltaic devices [8, 27]; however, by the incident of photons and incorporation of In_2O_3 with TiO_2, the nanostructures boost up the photoexcited *e–h* pairs due to several scattering processes, which lead to increase the device efficiency. Here, we have reported an efficient photovoltaic device for UV region by depositing Ag nanoparticles on the top of TiO_2 and In_2O_3 thin films, where the Ag nanoparticles enhanced the quantum efficiency of the device by coupling incident light into guided modes through LSPR effect. The device is fabricated using the SS-GLAD technique, without the requirement of any annealing step which makes the device inexpensive, thereby making the device attractive for potential commercialization.

Experimental Process

Synthesis of In_2O_3/TiO_2 Thin Film

ITO-coated glass substrate (99.999% pure, MTI Corporation, USA) was cleaned using methanol, acetone, and deionized water. For further cleaning, the substrates were dipped into a mixed solution of hydrofluoric acid and deionized water with a dilution ratio of 1:50. A dense thin film (~100 nm) of TiO_2 has been synthesized upon pre-cleaned ITO-coated glass substrate using an electron beam evaporator (e-beam) (HHV Co. (p) Ltd., Model-15F6) technique with a base pressure of 0.05 mbar. A high vacuum chamber pressure of ~0.2×10^{-4} mbar and deposition rate of 1.2×10^{-10} m/s was maintained during the synthesis of TiO_2 thin film. The film substrate holder was held at a perpendicular distance of ~ 16 cm from the evaporated material source. A similar technique has been followed to synthesize the In_2O_3 thin film (~100 nm) over the TiO_2 thin film at a deposition rate of 0.5×10^{-10} m/s.

Fabrication of Ag Nanoparticles

SS-GLAD technique has been carried out to fabricate the Ag (highly pure 99.999%) nanoparticles over In_2O_3/TiO_2 thin film. The crucible filled with Ag pellets was placed at a vertical distance of < 30 cm from the substrate holder with an azimuthal angle and a spin of 85° and 460 rpm, respectively. A deposition rate of 1.2×10^{-10} m/s was maintained during the fabrication of Ag nanoparticles, as well.

Device Fabrication

To fabricate the device, indium (In) (99.999% pure beads, MTI Corporation, USA) has been deposited on the samples through an aluminium mask hole (each hole diameter ~1.95×10^{-6} m^2), which act as the electrode for the device. Here two distinct devices, viz., In_2O_3/TiO_2 thin film and In_2O_3/TiO_2 thin film/Ag nanoparticles, were fabricated, as shown in Fig. 1a, b, respectively.

Characterizations

FESEM and EDAX has been done to morphologically characterize the samples using SIGMA-300 (Zeiss). The XRD was done on a Bruker D8 Advance diffractometer to study the structural characterization. The absorption, reflection and transmission spectrum were recorded by a

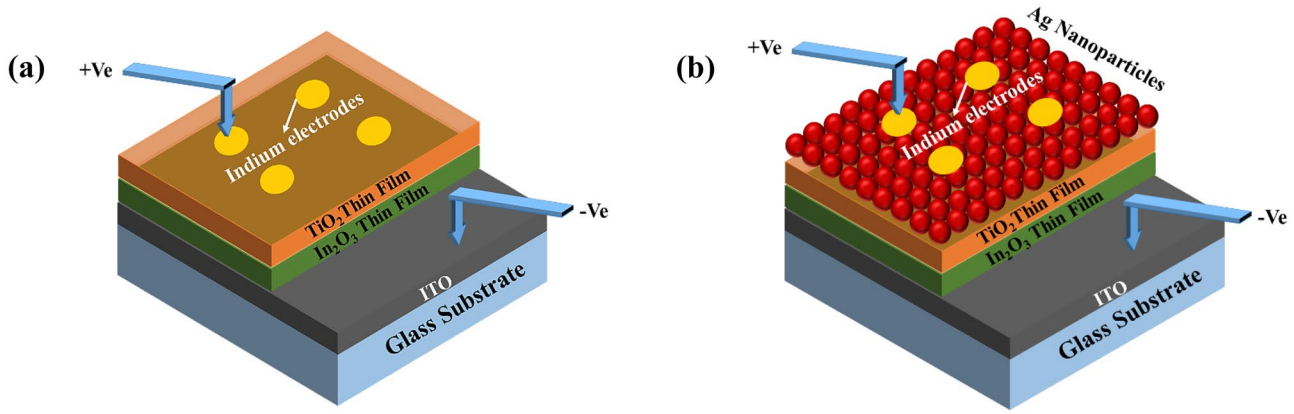

Fig. 1 Schematic diagram of the two fabricated devices. **a** In_2O_3/TiO_2 thin film. **b** In_2O_3/TiO_2 thin film/Ag nanoparticles

Perkin Elmer LAMBDA 950 UV–VIS-NIR Spectrophotometer. The electrical characteristics were investigated using a Keysight B2902A source and measurement units (SMUs).

Results and Discussions

Morphological Analysis of Fabricated Structures

The morphology of the fabricated thin film and nanoparticles were shown in Fig. 2a, b. Figure 2b shows the FESEM image of the In_2O_3/TiO_2 thin film/Ag nanoparticles sample using SS-GLAD technique, where the Ag nanoparticles were densely packed and randomly distributed all over the thin film surface. The growth of densely packed nanoparticles was aided by high substrate temperature in the vacuum chamber [36]. This technique is preferred here because of its highly user-friendly interface and easily controllable features (rotation speed, azimuthal angle, evaporation rate, substrate temperature, etc.) [37]. The particle size histogram (Fig. 2c) shows that the Ag nanoparticles range between ~4 and ~40 nm, and a huge percentage of the deposited particles had a diameter between ~7 and ~12 nm. Figure 2d shows the EDAX spectra of In_2O_3/TiO_2 thin film/Ag nanoparticles

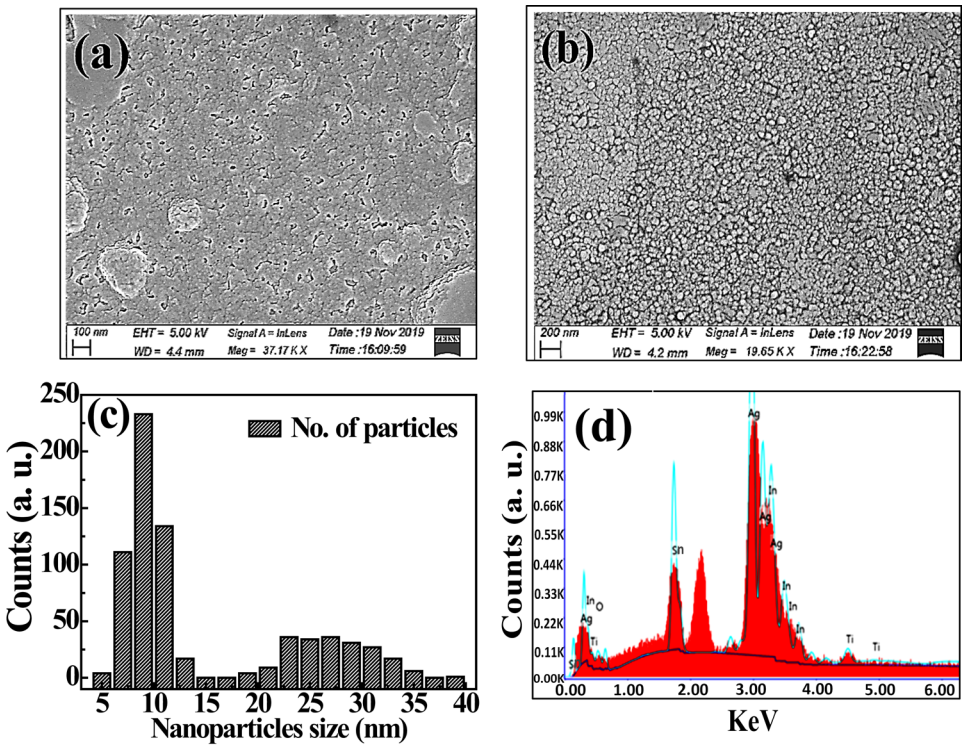

Fig. 2 Top view FESEM images of **a** In_2O_3/TiO_2 thin film and **b** In_2O_3/TiO_2 thin film/Ag nanoparticles. **c** Particle size histogram image of Ag nanoparticles. **d** EDAX analysis of the sample

Table 1 EDAX data

Element	Weight (%)	Atomic (%)	*K* ratio
O K	3.40	15.53	0.0042
Sn L	9.61	25.01	0.0659
Ag L	55.19	37.40	0.5226
In L	29.78	18.96	0.2568
Ti K	2.02	3.09	0.0160
Total	100.00		

sample, where the elemental composition of oxygen (O [K]), tin (Sn [L]), silver (Ag [L]), indium (In [L]), and titanium (Ti [K]) was detected. Table 1 lists the atomic and weight percentage of elements present in the sample.

Structural Analysis

More information about the phases, crystal orientations, and morphology of the In_2O_3/TiO_2 thin film and In_2O_3/TiO_2 thin film/Ag nanoparticles samples can be analyzed from XRD measurements, carried out using Bruker D8 Advanced using Cu-Kα target source under the diffraction angle (2θ) between 20° and 80°. Figure 3a shows the XRD peaks for In_2O_3/TiO_2 thin film. The peaks (211), (222), (431) corresponds to In_2O_3 (JCPDS card no. 06–0416) [38] and the peaks (103), (200), (220), (125) corresponds to TiO_2 anatase phase (JCPDS card no. 89–4921) [39]. The planes of (111), (200), (220), and (311) correspond to Ag peaks (JCPDS card no. 03–0921) [39] which were formed due to the deposition of Ag nanoparticles over the In_2O_3/TiO_2 thin film. Additionally, the peaks (031) and (242) corresponds to Ag_3O_4 monoclinic crystal structure (JCPDS card no. 84–1261) which is attributed to the formation of Ag–O compound [36] during fabrication. Dwivedi et al. [39], Xie et al. [40], and Laskri et al. [41] also reported such type of Ag–O compound during the synthesis of Ag nanoparticles. Therefore, the XRD patterns confirm the presence of In2O3, TiO2 and Ag in the fabricated samples.

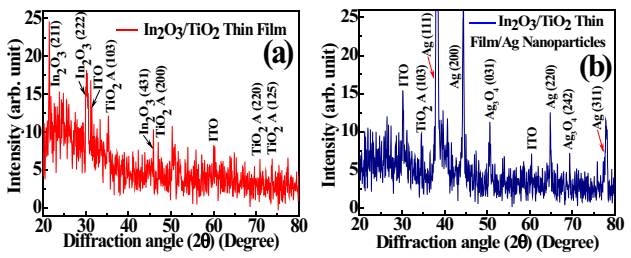

Fig. 3 XRD profiles for **a** In_2O_3/TiO_2 thin film and **b** In_2O_3/TiO_2 thin film/Ag nanoparticles

Optical Properties Analysis

Figure 4a shows the comparison of absorption spectra of In_2O_3/TiO_2 thin film with In_2O_3/TiO_2 thin film/Ag nanoparticles on ITO-coated glass substrate in the wavelength range of 200–800 nm. A ~45 nm red shift has been observed in the UV region for In_2O_3/TiO_2 thin film/Ag nanoparticles sample which may be the effect of localized surface plasmon resonance of Ag nanoparticles in the sample [42]. Under irradiation, the Ag nanoparticles exhibit a large electron oscillation and generated inorganic Ag–O compound, as previously explained in the "Structural Analysis" section. This inorganic Ag–O compound was generated due to localized surface plasmon and thus absorption of light in the UV region by the detector has been occurred. Figure 4b compares the measured reflectance of both samples using UV–Vis diffused reflectance spectroscopy (DRS), where In_2O_3/TiO_2 thin film/Ag nanoparticles exhibits a significantly lower reflectivity in the UV (~60%) and visible (~25%) region after applying only Ag nanoparticles on the seed layer (thin film). This dropping of reflectance can indicate the reduction of bandgap energy for the In_2O_3/TiO_2 thin film/Ag nanoparticles. To demonstrate the bandgap energy of the samples Kubelka–Munk function method [43]. According to the theory of P. Kubelka and F. Munk, the diffusive reflectance can be written as:

$$[F(R)] = \frac{K}{S} = \frac{(1-R)^2}{2R} \tag{1}$$

where "*R*" is the measured reflectance, "*K*" is the molar absorption coefficient, "*S*" is the scattering factor, "*h*" is the Planck's constant, and [F(*R*)] is known as the Kubelka–Munk function. In the plot, the linear extrapolation over the "$h\nu$" axis of $(F(R)h\nu)^2$ versus $h\nu$ gives the values of bandgap, where the bandgap energy of ~4.28 eV and ~4.16 eV was obtained and demonstrated in Fig. 4c for In_2O_3/TiO_2 thin film and In_2O_3/TiO_2 thin film/Ag nanoparticles, respectively. The reduction in bandgap energy is accredited to the red shift of Ag nanoparticles coated sample which is due to the trapped *e–h* recombination at the oxygen vacancies and electron transmission of Ag to the conduction band of the oxide thin films [44]. The optical transmittance spectra in Fig. 4d shows a ~90% transmittance in the UV region, for the In_2O_3/TiO_2 thin film/Ag nanoparticles as compared to ~50% of that of the In_2O_3/TiO_2 thin film. Hence, it proves that the light falls on the Ag nanoparticles surface completely gets transmitted completely by reducing the amount of reflection loss.

Moreover, the presence of oxygen vacancies leads to add the additional energy levels in the bandgap, known as the Urbach tail. The Urbach tails of the samples were characterized from the Urbach energy (E_U) (Eq. 2) plot with the incident photon energy.

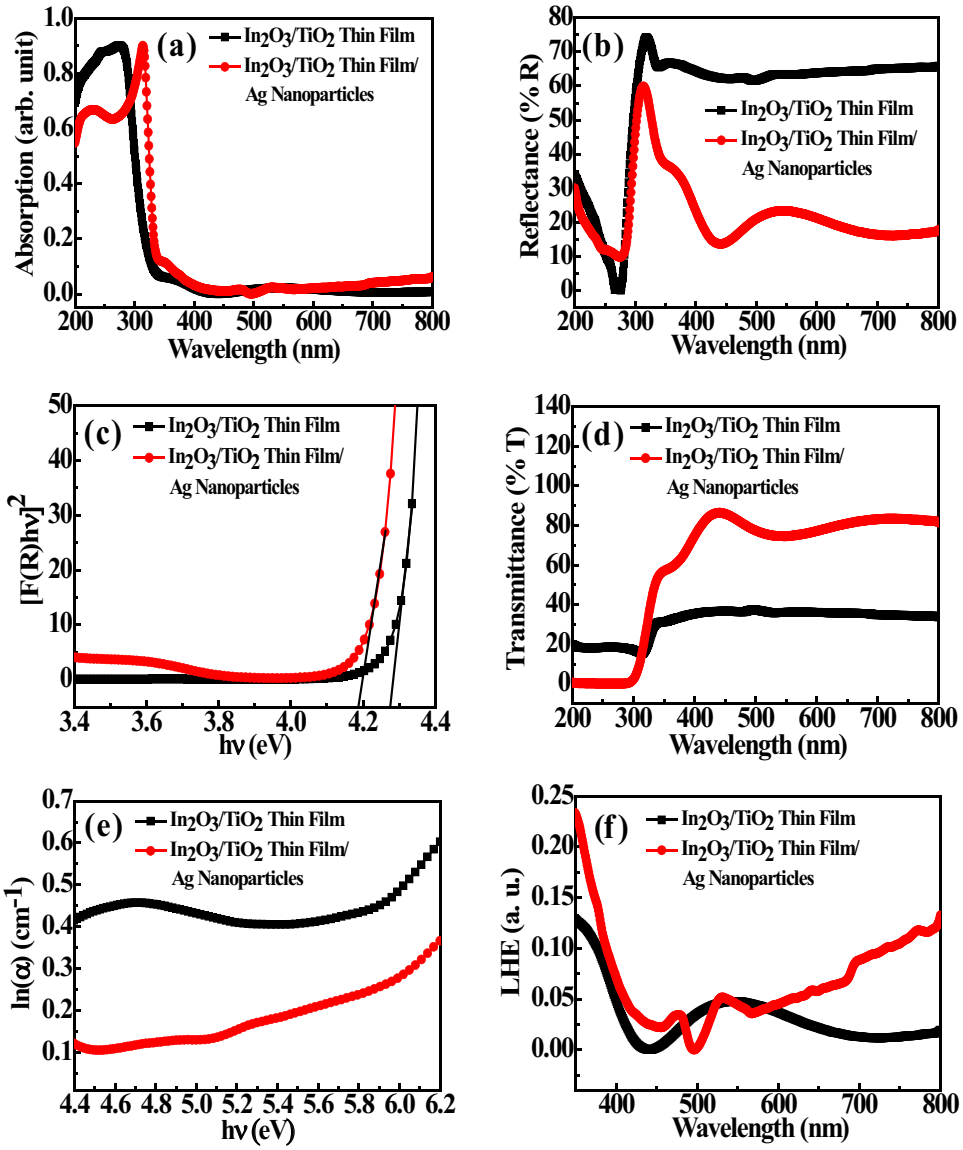

Fig. 4 **a** Absorption spectra. **b** UV-DRS spectra (reflectance spectra), **c** Kubelka–Munk plot (for bandgap), **d** Transmittance spectra, **e** Urbach energy, **f** Light harvesting efficiency (LHE) characteristics of In_2O_3/TiO_2 thin film and In_2O_3/TiO_2 thin film/Ag nanoparticles samples on a ITO-coated glass substrate

$$ln(\alpha) = ln(\alpha_0) + (\frac{h\nu}{E_U}) \tag{2}$$

where α is known as the absorption coefficient, α_0 is a constant, $h\nu$ is incident photon energy, and E_U is the Urbach energy [45, 46]. The E_U signifies the spread of defect energy states inside the bandgap. The E_U was also used to analyse the sample performance, since the E_U affects the carrier mobility, carrier lifetime, and cell performance [47]. The reciprocal of the slope value of the linear portion of $ln(\alpha)$ versus $h\nu$ shown in Fig. 4e was utilized to estimate E_U value. The calculated value of E_U was 3.45 eV and 4.90 eV for the In_2O_3/TiO_2 thin film and In_2O_3/TiO_2 thin film/Ag nanoparticles samples respectively. This enhancement in E_U was due to the presence of oxygen vacancies in the Ag nanoparticles decorated sample [48], which corroborates the previous UV analysis.

Figure 4f depicts the variation of light harvesting efficiency (LHE) for In_2O_3/TiO_2 thin film with In_2O_3/TiO_2 thin film/Ag nanoparticles samples between the wavelength ranges of 350–800 nm. Here, the enhanced LHE characteristics for In_2O_3/TiO_2 thin film/Ag nanoparticles samples suggests the enhanced light absorption due to the incorporation of Ag nanoparticles on the thin film samples [49]. According to the Beer-Lambert law, the LHE characteristics can be further enhanced by increasing the length of the optical path by modifying the nanocrystalline films [50]. The LHE characteristics can be obtained using Eq. (3).

$$\mathrm{LHE}(\lambda) = 1 - 10^{-ad} \tag{3}$$

where α and d is the absorption coefficient and thickness of the nanocrystalline film [49].

Analysis of Electrical Characteristics

The power conversion efficiency (η) of the In_2O_3/TiO_2 thin film/Ag nanoparticles device and the In_2O_3/TiO_2 thin film device need to be characterized. For this purpose, the photovoltaic parameters, namely open circuit voltage (V_{OC}), short circuit photocurrent density (J_{SC}), and fill factor (FF) were obtained. Figure 5a shows the experimental setup for the measurement of photovoltaic parameters, where a tungsten filament source is illuminating the fabricated devices at room temperature. A B2902A source and measurement unit (SMU) has been used for recording the characteristics. The obtained *J-V* curve for In_2O_3/TiO_2 thin film and In_2O_3/TiO_2 thin film/Ag nanoparticles devices, were plotted in Fig. 5b. Table 2 lists the corresponding measured photovoltaic parameters considering an effective device area of 1.8 mm^2 for both the devices.

It has been found that the maximum current that the device can deliver, i.e., the short circuit photocurrent density (J_{SC}), or the current that flows in the circuit when the electrodes are shorted, was enhanced by ~136% for the In_2O_3/TiO_2 thin film/Ag nanoparticles device compared to that of the In_2O_3/TiO_2 thin film. The maximum voltage delivered by the device or open circuit voltage (V_{OC}), also increases for the In_2O_3/TiO_2 thin film/Ag nanoparticles device. The fill factor (FF) which is the ratio between the maximum power of the device and the product of V_{OC} and J_{SC} has been found to be 58% and 53% for the In_2O_3/TiO_2 thin film/Ag nanoparticles device and the In_2O_3/TiO_2 thin film device, respectively. All these parameters leads to an increase of ~127 times enhancement in the power conversion efficiency (PCE) for the In_2O_3/TiO_2 thin film/Ag nanoparticles device (15.12%) compared to the In_2O_3/TiO_2 thin film device (11.90%). This significant enhancement in efficiency is attributed due to the LSPR effect, introduced by the depositing plasmonic Ag nanoparticles [49].

Table 2 Photovoltaic parameters for the two device structures

Device structure	V_{OC} (V)	J_{SC} (μA/cm^2)	FF (%)	η (%)
ITO/In_2O_3/TiO_2 thin film	0.88	22.9	58	11.90
ITO/In_2O_3/TiO_2 thin film/ Ag nanoparticles	0.91	31.1	53	15.12

The overall PCE (η) was estimated at room temperature from the short circuit photocurrent density (J_{SC}), open circuit voltage (V_{OC}), and the fill factor of the sample (FF) to the power of the incident light (P_{light}), as given by the Eq. (4) [51].

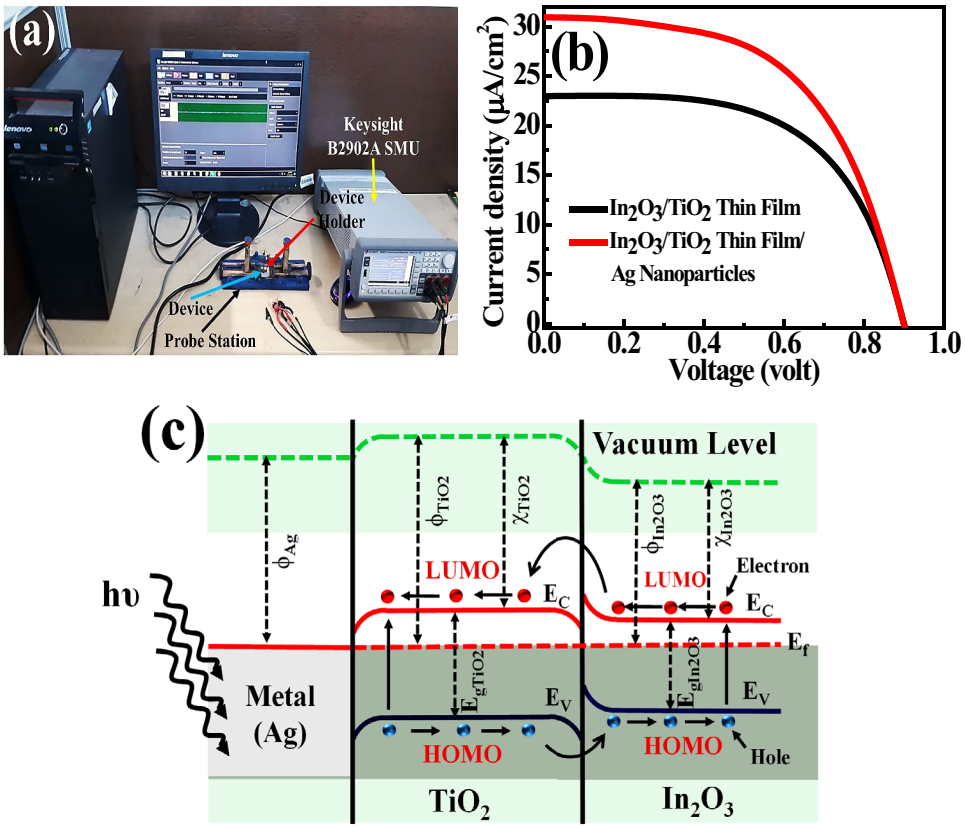

Fig. 5 **a** Experimental setup for the measurement of photovoltaic parameters. **b** *J-V* curve for In_2O_3/TiO_2 thin film and In_2O_3/TiO_2 thin film/Ag nanoparticles devices. **c** A schematic illustration of the staggered gap diagram

Table 3 Comparison of state of the art of this work with other reported work

Sl. no	Device name	FF (%)	η (%)	References
1	Ag NPs textured In_2O_3/TiO_2 thin films	53	15.12	[This work]
2	TiO_2 photoelectrode morphology of N719 DSSC	74.1	9.8	[52]
3	In_2O_3/CdS/$CulnS_2$ thin-film solar cell	61	9.7	[53]
4	n-AZO nanorod solar cell	39.38	6.25	[54]
5	Dye sensitized nanocrystalline TiO_2 solar cell	63	5.6	[55]
6	nb-doped TiO_2/Sn-doped In_2O_3 multi-layered DSSC	70.9	5.13	[56]
7	Mn dopant in CdS quantum dot sensitized solar cell	55	3.29	[57]
8	Nanoporous TiO_2 film based DSSC	60	2.87	[58]
9	SnO_2 photoanode treated with $TiCl_4$	57	2.85	[59]
10	ZnO nanoparticles based dye-sensitized solar cells	48.5	1.97	[60]

$$\%\mathrm{PCE}(\eta) = \frac{(J_{SC}V_{OC}FF)}{P_{light}} \tag{4}$$

where the FF was determined from the ratio of maximum power (P_{max}) of the samples per unit area to the V_{OC} and J_{SC} [51].

$$\mathrm{FF} = \frac{P_{max}}{(V_{OC}J_{SC})} \tag{5}$$

Figure 5c shows the staggered gap diagram of the In_2O_3/TiO_2 thin film/Ag nanoparticles device, where Φ and χ is the work function and electron affinity of Ag NPs, TiO_2, and In_2O_3, respectively. When the light ($h\upsilon$) is illuminated on the device, electrons are excited state from the highest occupied molecular orbital (HOMO) to the lowest unoccupied molecular orbital (LUMO) [51], which are then collected. The Ag nanoparticles increases the photon path which leads to higher conversion efficiencies. Table 3 depicts the comparison of state of the art of this work with other reported work based on the device performances. Therefore, a low-cost SS-GLAD technique of fabricating high efficiency solar cells which are aided by the LSPR effect of the deposited Ag nanoparticles has been studied. The fabrication step does not require further processing steps after SS-GLAD which makes the device inexpensive, thereby making the device attractive for potential commercialization.

Conclusion

A thorough analysis were done for In_2O_3/TiO_2 thin film and In_2O_3/TiO_2 thin film/Ag nanoparticles samples to inspect the morphological, structural and optical characteristics. The marginal optical bandgap energy (~4.16 eV), high transmittance (~90%), low reflectance in UV (~60%), and visible (~25%) region, Jsc of 31.1 mA/cm^2, Voc of 0.91 V, FF of 53%, and PCE of 15.12% was observed for In_2O_3/TiO_2 thin film/Ag nanoparticles as compared to the In_2O_3/TiO_2 thin film. Therefore, the use of Ag nanoparticles textured oxide thin film–based device is a promising approach for the photovoltaic applications.

Acknowledgements The authors are acknowledged to Central Instrumentation Centre, Tripura University, INDIA for providing FESEM and EDAX facility. The authors also acknowledged to SAIF, IIT Madras for optical measurement facility. The authors thankful to Dr. B. Saha, Assistant Professor, Department of Physics, NIT Agartala, INDIA for providing the XRD measurement facility.

Author Contribution Amitabha Nath: methodology, device fabrication, electrical measurements, data analysis, writing—original draft. Naveen Bhati: characterizations and data analysis. Bikram Kishore Mahajan: analysis, writing and editing. Jayanta Kumar Rakshit: validation and editing. Mitra Barun Sarkar: conceptualization, validation, editing and supervision.

Data Availability The materials described in the manuscript, including all relevant raw data, will be freely available from the corresponding author upon reasonable request.

Declarations

Ethics Approval I have followed the ethical principles and accurate references to scientific sources in my original article.

Consent to Participate Informed consent was obtained from all authors.

Consent for Publication I consent to the publication of my original research article.

Conflict of Interest The authors declare no competing interests.

References

1. Bertoluzzi L, Ma S (2012) On the methods of calculation of the charge collection efficiency of dye sensitized solar cells. Phys Chem Chem Phys 15(12):4283–4285. https://doi.org/10.1039/c3cp44248a
2. Gratzel M (2005) Solar energy conversion by dye-sensitized photovoltaic cells. Inorg Chem 44(20):6841–6851. https://doi.org/10.1021/ic0508371

3. Katoh R, Furube A (2014) Electron injection efficiency in dye-sensitized solar cells. J Photochem Photobiol C 20:1–16. https://doi.org/10.1016/j.jphotochemrev.2014.02.001
4. Liu M, Johnston MB, Snaith HJ (2013) Efficient planar heterojunction perovskite solar cells by vapour deposition. Nature 501(7467):395–398. https://doi.org/10.1038/nature12509
5. Park NG (2015) Perovskite solar cells: an emerging photovoltaic technology. Mater Today 18(2):65–72. https://doi.org/10.1016/j.mattod.2014.07.007
6. Wu R, Yang Y, Li M, Qin D, Zhang Y, Hou L (2017) Solvent engineering for high-performance PbS quantum dots solar cells. Nanomaterials 7(8):201(1–13). https://doi.org/10.3390/nano7080201
7. Wang Z, Hu Z, Kamarudin MA, Kapil G, Tripathi A, Shen Q, Yoshino K, Minemoto T, Pandey SS, Hayase S (2018) Enhancement of charge transport in quantum dots solar cells by *N*-butylamine-assisted sulfur-crosslinking of PbS quantum dots. Sol Energy 174:399–408. https://doi.org/10.1016/j.solener.2018.09.026
8. Yu P, Zhu K, Norman AG, Ferrere S, Frank AJ, Nozik AJ (2006) Nanocrystalline TiO_2 Solar Cells Sensitized with InAs Quantum Dots. J Phys Chem B 110(50):25451–25454. https://doi.org/10.1021/jp064817b
9. Shrotriya V, Li G, Yao Y, Moriarty T, Emery K, Yang Y (2006) accurate measurement and characterization of organic solar cells. Adv Funct Mater 16(15):2016–2023. https://doi.org/10.1002/adfm.200600489
10. Morel DL, Ghosh AK, Feng T, Stogryn EL, Purwin PE (1978) High efficiency organic solar cells. Appl Phys Lett 32(8):495–497. https://doi.org/10.1063/1.90099
11. Stuart HR, Hall DG (1996) Absorption enhancement in silicon on insulator waveguides using metal island films. Appl Phys Lett 69(16):2327–2339. https://doi.org/10.1063/1.117513
12. Deng Y, Cao G, Yang H, Zhou X, Wu Y (2018) Dynamic control of double plasmon-induced transparencies in aperture-coupled waveguide-cavity system. Plasmonics 13(1):345–352. https://doi.org/10.1007/s11468-017-0519-z
13. Deng Y, Cao G, Wu Y, Zhou X, Liao W (2015) Theoretical description of dynamic transmission characteristics in MDM waveguide aperture-side-coupled with ring cavity. Plasmonics 10(6):1537–1543. https://doi.org/10.1007/s11468-015-9971-9
14. Cao G, Li H, Deng Y, Zhan S, He Z, Li B (2014) Systematic theoretical analysis of selective-mode plasmonic filter based on aperture-side-coupled slot cavity. Plasmonics 9(5):1163–1169. https://doi.org/10.1007/s11468-014-9727-y
15. Said DA, Ali AM, Khayyat MM, Boustimi M, Loulou M, Seoudi R (2019) A study of the influence of plasmonic resonance of gold nanoparticle doped PEDOT: PSS on the performance of organic solar cells based on CuPc/$C6_0$. Heliyon 5(11):e02675. https://doi.org/10.1016/j.heliyon.2019.e02675
16. Notarianni M, Vernon K, Chou A, Aljada M, Liu J, Motta N (2014) Plasmonic effect of gold nanoparticles in organic solar cells. Sol Energy 106:23–37. https://doi.org/10.1016/j.solener.2013.09.026
17. Su YH, Ke YF, Cai SL, Yao QY (2012) Surface plasmon resonance of layer-by-layer gold nanoparticles induced photoelectric current in environmentally-friendly plasmon-sensitized solar cell. Light Sci Appl 1(6):e14. https://doi.org/10.1038/lsa.2012.14
18. Baryshnikova KV, Petrov MI, Babicheva VE, Belov PA (2016) Plasmonic and silicon spherical nanoparticle antireflective coatings. Sci Rep 6:22136(1–11). https://doi.org/10.1038/srep22136
19. Lesina AC, Paternoster G, Mattedi F, Ferrario L, Berini P, Ramunno L, Paris A, Vaccari A, Calliari L (2015) Modeling and characterization of antireflection coatings with embedded silver nanoparticles for silicon solar cells. Plasmonics 10(6):1525–1536. https://doi.org/10.1007/s11468-015-9957-7
20. Singh HK, Sandeep K, Chary M, Balraj A, Sharma P, Solanki CS (2014) Investigation on silver nanoparticles-based plasmonic antireflection and its impact on electrical performance of mono c-Si solar cells. 2014 IEEE 2nd International Conference on Emerging Electronics (ICEE) 1–4. https://doi.org/10.1109/ICEmElec.2014.7151167
21. Zhang Y, Cai B, Jia B (2016) Ultraviolet plasmonic aluminium nanoparticles for highly efficient light incoupling on silicon solar cells. Nanomaterials 6(6):95(1–10). https://doi.org/10.3390/nano6060095
22. Parashar PK, Sharma RP, Komarala VK (2016) Plasmonic silicon solar cell comprised of aluminum nanoparticles: effect of nanoparticles' self-limiting native oxide shell on optical and electrical properties. J Appl Phys 120(14):143104–1–143104–9. https://doi.org/10.1063/1.4964869
23. Temple TL, Bagnall DM (2011) Optical properties of gold and aluminium nanoparticles for silicon solar cell applications. J Appl Phys 109(8):084343–1–084343–1. https://doi.org/10.1063/1.3574657
24. Wu X, Liu P, Ma L, Zhou Q, Chen Y, Lu J, Yang S (2016) Two-dimensional modelling of TiO_2 nanowire based organic–inorganic hybrid perovskite solar cells. Sol Energy Mater Sol Cells 152:111–117. https://doi.org/10.1016/j.solmat.2016.03.017
25. Wang YC, Chen CY, Kuo CW, Kuan TM, Yu CY, Chen IC (2016) Low-temperature grown indium oxide nanowire-based antireflection coatings for multi-crystalline silicon solar cells. Phys Status Solidi 213(8):2259–2263. https://doi.org/10.1002/pssa.201600005
26. Leem DS, Edwards A, Faist M, Nelson J, Bradley Donal DC, de Mello JC (2011) Efficient organic solar cells with solution-processed silver nanowire electrodes. Adv Mater 23(38):4371–4375. https://doi.org/10.1002/adma.201100871
27. Parayil SK, Lee YM, Yoon M (2009) Photoelectrochemical solar cell properties of heteropolytungstic acid-incorporated TiO_2 nanodisc thin films. Electrochem commun 11(6):1211–1216. https://doi.org/10.1016/j.elecom.2009.04.031
28. Rockstuhl C, Lederer F (2009) Photon management by metallic nanodiscs in thin film solar cells. Appl Phys Lett 94(21):213102–1–213102–3. https://doi.org/10.1063/1.3141402
29. Ali M, Zhou F, Chen K, Kotzur C, Xiao C, Bourgeois L, Zhang X, MacFarlane DR (2016) Nanostructured photoelectrochemical solar cell for nitrogen reduction using plasmon-enhanced black silicon. Nat Commun 7:11335(1–5). https://doi.org/10.1038/ncomms11335
30. Luther JM, Law M, Beard MC, Song Q, Reese MO, Ellingson RJ, Nozik AJ (2008) Schottky Solar Cells Based on Colloidal Nanocrystal Films. Nano Lett 8(10):3488–3492. https://doi.org/10.1021/nl802476m
31. Ergen O, Gibb A, Vazquez-Mena O, Regan WR, Zettl A (2015) Metal insulator semiconductor solar cell devices based on a Cu_2O substrate utilizing h-BN as an insulating and passivating layer. Appl Phys Lett 106(10):103904–1–103904–4. https://doi.org/10.1063/1.4914181
32. Shewchun J, Burk D, Spitzer MB (1980) MIS and SIS solar cells. IEEE Trans Electron Devices 27(4):705–716
33. Su J, Yang H, Xu Y, Tang Y, Yi Z, Zheng F, Zhao F, Liu L, Wu P, Li H (2021) Based on ultrathin PEDOT:PSS/c-Ge solar cells design and their photoelectric performance. Coatings 11(7):748(1–12). https://doi.org/10.3390/coatings11070748
34. Zhao F, Chen X, Yi Z, Qin F, Tang Y, Yao W, Zhou Z, Yi Y (2020) Study on the solar energy absorption of hybrid solar cells with trapezoidpyramidal structure based PEDOT:PSS/c-Ge. Sol Energy 204:635–643. https://doi.org/10.1016/j.solener.2020.05.030
35. Sarkar MB, Choudhuri B, Bhattacharya P, Barman RN, Ghosh A, Dwivedi SMMD, Chakrabartty S, Mondal A (2018) Improved UV photodetection by indium doped TiO_2 thin film based photodetector. J Nanosci Nanotechnol 18(7):4898–4903. https://doi.org/10.1166/jnn.2018.15295

36. Nath A, Sarkar MB (2021) Surface-plasmon-induced Ag nanoparticles decorated In_2O_3 nanowires for low noise photodetectors. Plasmonics 16(1):37–48. https://doi.org/10.1007/s11468-020-01262-z
37. Nath A, Raman R, Singh LR, Sarkar MB (2021) Enhanced photodetection in glancing angle deposited one-dimensional In_2O_3 nanorod array. J Nanosci Nanotechnol 21(5):3115–3122. https://doi.org/10.1166/jnn.2021.19280
38. Anand K, Kaur J, Singh RC, Thangaraj R (2016) Structural, optical and gas sensing properties of pure and Mn-doped In_2O_3 nanoparticles. Ceram Int 42(9):10957–10966. https://doi.org/10.1016/j.ceramint.2016.03.233
39. Dwivedi SMMD, Ghosh A, Deepthy S, Maji M, Lahiri R, Mondal S, Ghosh C, Dalal A, Mondal A, Ghosh M (2020) Detection technique for vitamin D_3 using Er-doped TiO_2 nanowire-based UV photodetector. J Nanophoton 14(4):046001–1–046001–17. https://doi.org/10.1117/1.JNP.14.046001
40. Xie W, Li Y, Sun W, Huang J, Xie H, Zhao X (2010) Surface modification of ZnO with Ag improves its photocatalytic efficiency and photostability. J Photochem Photobiol, A 216(2–3):149–155. https://doi.org/10.1016/j.jphotochem.2010.06.032
41. Laskri A, Drici A, Boulouma A, Amara A, Bernede JC (2019) Investigation of microstructural and optical properties of Ag3O4 thin films sprayed onto glass substrate. J Nano R 58:90–101. https://doi.org/10.4028/www.scientific.net/JNanoR.58.90
42. Nath A, Raman R, Yadav VK, Sannibabu P, Sarkar MB (2020) Bandgap modulation of glancing angle deposition aided Ag nanoparticles covered TiO_2 thin film by high temperature annealing. J Nanosci Nanotechnol 20(12):7636–7643. https://doi.org/10.1166/jnn.2020.18575
43. Kubelka P (1947) New contributions to the optics of intensely light-scattering materials. Part I J Opt Soc Am 38(5):448–457. https://doi.org/10.1364/JOSA.38.000448
44. Shin SG, Choi HW (2020) Improvement of characteristics of metal doped TiO_2 thin film and application to perovskite solar cell. J Nanosci Nanotechnol 20(11):7130–7134. https://doi.org/10.1166/jnn.2020.18846
45. Nath A, Mahajan BK, Singh LR, Vishwas S, Nanda RK, Sarkar MB (2021) Enhancing detectivity of indium-oxide-based photodetectors via vertical nanostructuring through glancing angle deposition. J Electron Mater 1–9. https://doi.org/10.1007/s11664-021-08889-6
46. Hassanien AS, Akl AA (2015) Influence of composition on optical and dispersion parameters of thermally evaporated non-crystalline $Cd_{50}S_{50-x}Se_x$ thin films. J Alloys Compd 648:280–290. https://doi.org/10.1016/j.jallcom.2015.06.231
47. Chantana J, Nishimura KY, Teraji S, Watanabe T, Minemoto T (2019) Examination of relationship between Urbach energy and open-circuit voltage deficit of flexible Cu(In, Ga)Se solar cell for its improved photovoltaic performance. ACS Appl Energy Mater 2(11):7843–7849. https://doi.org/10.1021/acsaem.9b01271
48. Chen Y, Xu XL, Zhang GH, Xue H, Ma SY (2009) A comparative study of the microstructures and optical properties of Cu- and Ag-doped ZnO thin films. Phys B 404(20):3645–3649. https://doi.org/10.1016/j.physb.2009.06.051
49. Zhao H, Huang F, Hou J, Liu Z, Wu Q, Cao H, Jing Q, Peng S, Cao G (2016) Efficiency enhancement of quantum dot sensitized TiO_2/ZnO nanorod arrays solar cells by plasmonic Ag nanoparticles. ACS Appl Mater Interfaces 8(40):26675–26682. https://doi.org/10.1021/acsami.6b06386
50. Tachibana Y, Hara K, Sayama K, Arakawa H (2002) Quantitative analysis of light-harvesting efficiency and electron-transfer yield in ruthenium-dye-sensitized nanocrystalline TiO_2 solar cells. Chem Mater 14(6):2527–2535. https://doi.org/10.1021/cm011563s
51. Saravanan S, Kato R, Balamurugan M, Kaushik S, Soga T (2017) Efficiency improvement in dye sensitized solar cells by the plasmonic effect of green synthesized silver nanoparticles. J Sci: Adv Mater Dev 2(4):418–424. https://doi.org/10.1016/j.jsamd.2017.10.004
52. Wang ZS, Kawauchi H, Kashima T, Arakawa H (2004) Significant influence of TiO_2 photoelectrode morphology on the energy conversion efficiency of N719 dye-sensitized solar cell. Coord Chem Rev 248(13–14):1381–1389. https://doi.org/10.1016/j.ccr.2004.03.006
53. Ogawa Y, Jäger-Waldau A, Hashimoto Y, Ito K (1994) In_2O_3/CdS/$CuInS_2$ thin-film solar cell with 9.7% efficiency. Jpn J Appl Phys 33(Part 2, No. 12B):L1775–L1777. https://doi.org/10.1143/JJAP.33.L1775
54. Sharma JR, Das G, Roy AB, Bose S, Mukhopadhyay S (2020) Design analysis of heterojunction solar cells with aligned AZO nanorods embedded in p-type Si wafer. Silicon 12(2):305–316. https://doi.org/10.1007/s12633-019-00134-4
55. Hara K, Sayama K, Ohga Y, Shinpo A, Suga S, Arakawa H (2001) A coumarin-derivative dye sensitized nanocrystalline TiO_2 solar cell having a high solar-energy conversion efficiency up to 5.6%. Silicon 6:569–570. https://doi.org/10.1039/b010058g
56. Kim DH, Lee S, Park JH, Noh JH, Park IJ, Seong WM, Hong KS (2011) Transmittance optimized nb-doped TiO_2/Sn-doped In_2O_3 multilayered photoelectrodes for dye-sensitized solar cells. Sol Energy Mater Sol Cells 96:276–280. https://doi.org/10.1016/j.solmat.2011.09.011
57. Shen T, Tian J, Lv L, Fei C, Wang Y, Pullerits T, Cao G (2016) Investigation of the role of Mn dopant in CdS quantum dot sensitized solar cell. Electrochim Acta 191:62–69. https://doi.org/10.1016/j.electacta.2016.01.056
58. Saha S, Das P, Chakraborty AK, Sarkar S, Debbarma R (2016) Fabrication of DSSC with nanoporous TiO_2 film and Kenaf Hibiscus dye as sensitizer. Int J Renew Energy Res 6(2):1–8
59. Basu K, Benetti D, Zhao H, Jin L, Vetrone F, Vomiero A, Rosei F (2016) Enhanced photovoltaic properties in dye sensitized solar cells by surface treatment of SnO_2 photoanodes. Sci Rep 6(1):23312(1–10). https://doi.org/10.1038/srep23312
60. Shashanka R, Esgin H, Yilmaz VM, Caglar Y (2020) Fabrication and characterization of green synthesized ZnO nanoparticle based dye-sensitized solar cells. J Sci: Adv Mater Dev 5(2):185–191. https://doi.org/10.1016/j.jsamd.2020.04.005